On spreading of Antarctic Bottom Water in fracture zones of the Mid-Atlantic Ridge at 7–8°N

I. Yu. Dudkov[1,2], M. V. Kapustina[1], and V. V. Sivkov[1,2]

Received 9 Oct. 2021; accepted 26 May 2022; published 24 September 2022.

A Data-Interpolating Variational Analysis in n-dimensions was used to describe a potential temperature distribution in the bottom layer of the fracture zones of the Mid-Atlantic Ridge at 7–8°N. This analysis was based on a new digital terrain model obtained by supplementing the STRM15+ bathymetry data with multibeam echo sounding data from the 33rd cruise of the research vessel *Akademik Nikolaj Strakhov* (2016) and oceanological data from the World Ocean Database, supplemented with CTD profiles and reversing thermometer data measured in scientific cruises of the Shirshov Institute of Oceanology, Russian Academy of Sciences in 2014–2016. A 2D model of near-bottom potential temperature distribution in the study area was calculated based on the analysis. The model allows us to propose the Antarctic Bottom Water propagation pattern through the Doldrums, Vernadsky, and Pushcharovsky fracture zones. It is shown that bottom water warms up when passing fracture zones from 1.4°C in Pushcharovsky Fracture Zone up to 1.6–1.7°C in Vernadsky Fracture Zone. Bottom water from Pushcharovsky and Vernadsky fractures propagates in two directions. Northernly, it propagates to the Doldrums Fracture Zone, where its temperature reaches about 1.9–2.0°C. Easterly, it flows along Pushcharovsky Fracture Zone and raising the temperature up to 1.8–2.0°C. We propose the absence of Antarctic Bottom Water's overflow with a temperature less than 1.8°C to the East Atlantic in the study area. *KEYWORDS:* Antarctic Bottom Water; Mid-Atlantic Ridge; fracture zones; bottom topography; multibeam echo sounding; potential temperature.

Citation: Dudkov, I. Yu., M. V. Kapustina, and V. V. Sivkov (2022), On spreading of Antarctic Bottom Water in fracture zones of the Mid-Atlantic Ridge at 7–8°N, *Russ. J. Earth. Sci., 22,* ES5001, doi:10.2205/2022ES000783.

Introduction

Antarctic Bottom Water (AABW) is the densest of the deep-water masses in the open ocean. The main region of AABW formation is the Weddell Sea shelf. Leaving the shelf, AABW flows into the South Atlantic through the South Sandwich Trench and the Scotia Sea [*Seabrooke et al.,* 1971]. Here it is modified, mixing with the deep waters originating elsewhere on the Antarctic shelf and the deep circumpolar current. This mixing leads to a temperature gain of about 1°C [*Morozov et al.,* 2010].

Leaving the Scotia Sea, AABW enters the Argentine Basin through two deep passages: the Georgia Passage [*Locarnini et al.,* 1993] and the Shag Rocks Passage. Further, it propagates to the Brazil Basin through the Vema Channel [*Morozov and Tarakanov,* 2014] where, after overflowing the channel sill, it spreads almost to the entire Atlantic Ocean basins [*Morozov et al.,* 2010, 2021; *Whitehead and Worthington,* 1982].

AABW enters the East Atlantic basins through the fracture zones of the Mid-Atlantic Ridge (MAR), mainly the Romanche Fracture Zone (FZ), the Chain FZ [*Demidov et al.,* 2011; *Frey et al.,*

[1]Shirshov Institute of Oceanology RAS, Moscow, Russia
[2]Immanuel Kant Baltic Federal University, Kaliningrad, Russia

http://rjes.wdcb.ru/doi/2022ES000783-res.html

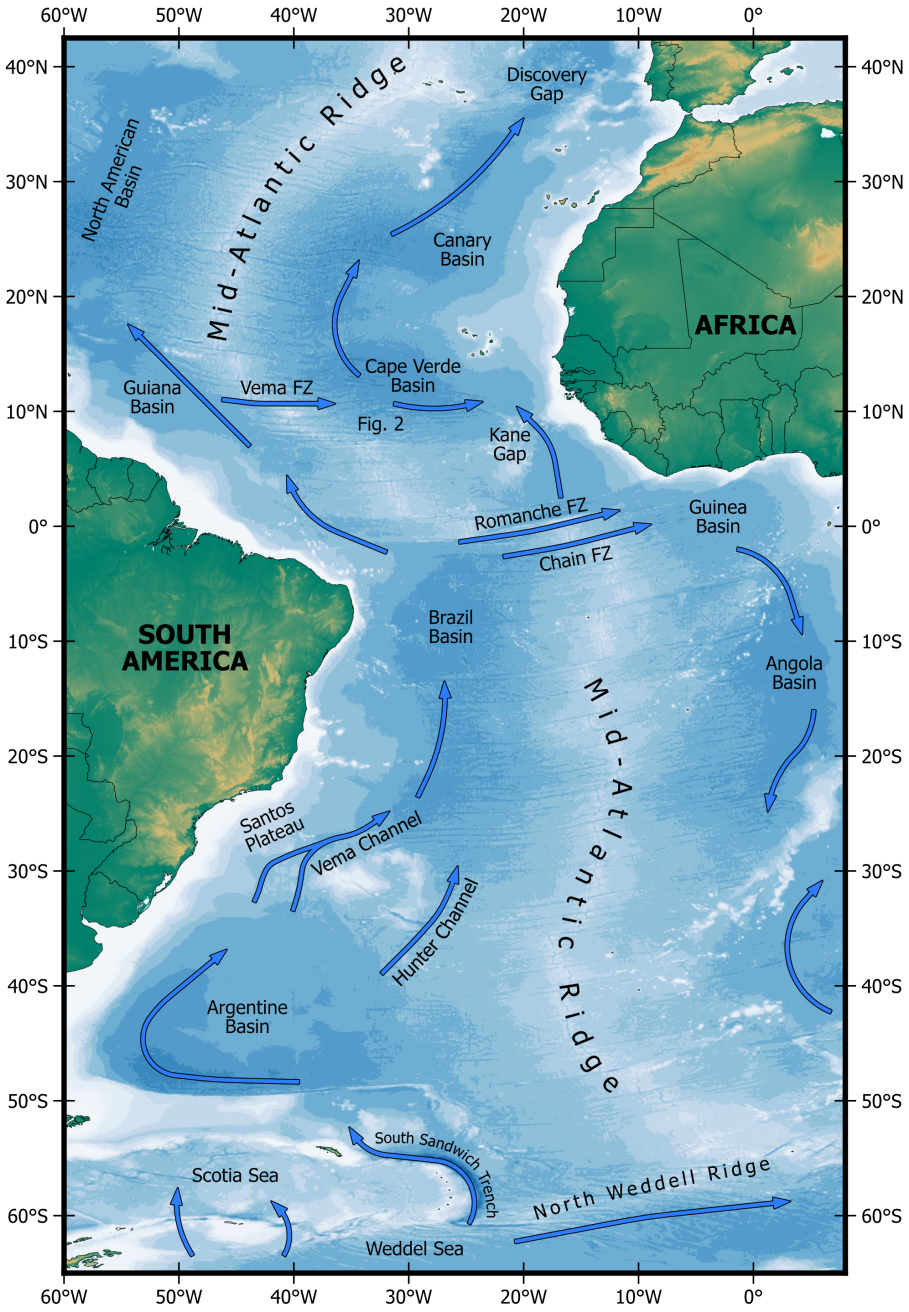

Figure 1. A general scheme of the AABW propagation in the Atlantic Ocean (after [*Morozov et al.*, 2010, 2012 2017]). Bottom topography from [*Tozer et al.*, 2019]. The red square displays the study area boundaries.

2019; *Mercier and Morin*, 1997; *Mercier and Speer*, 1998] and the Vema FZ [*Vangriesheim*, 1980] (Figure 1). Following from this, minor fractures zones are also interesting as AABW pathways, including: Doldrums, Vernadsky, Pushcharovsky (prior to 2020, a nameless fracture at 7°28′ N [*Morozov et al.*, 2017; *Pushcharovsky and Raznitsin*, 1991]), Bogdanov, and Strakhov [*Morozov et al.*, 2017].

The first evidence of possible AABW flow through the fracture zones at 7–8°N was found during the 39th–41st cruises of the research vessel (R/V) *Akademik Sergey Vavilov* in 2014–2016 [*Morozov et al.*, 2018]. These studies included CTD (conductivity, temperature, and pressure) and ADCP (water current velocity) profiling at several oceanographic stations. However, while

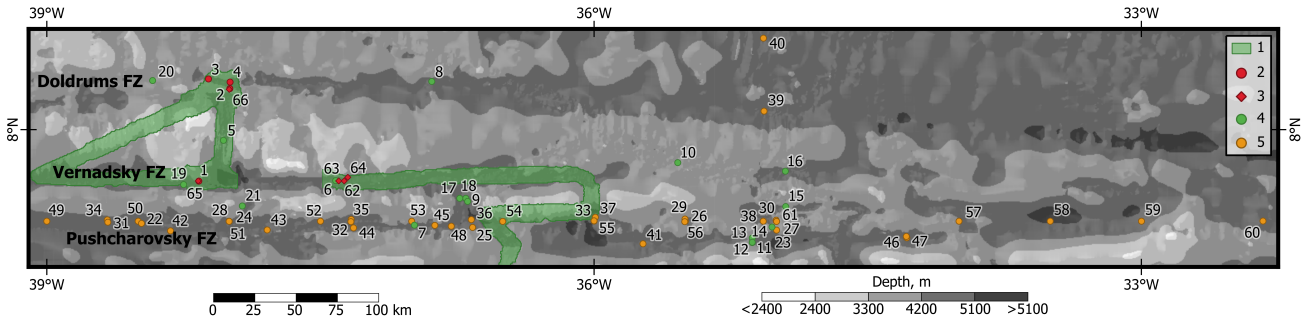

Figure 2. Study area. 1 – MBES survey site; 2 – CTD stations and 3 – high-precision thermometer measurements stations made in 2016 in the 33rd cruise of the R/V *Akademik Nikolaj Strakhov*; 4 – CTD stations made in 2014–2016 in the 39th–41st cruises of the R/V *Akademik Sergey Vavilov*; 5 – CTD stations from the WOD18. Bathymetry from [*Tozer et al.*, 2019].

it is widely known that bottom topography plays a key role in the propagation of bottom water [*Rhein et al.*, 1998], previous studies in the 7–8°N region do not factor in the effect of bottom topography. Given that consideration of the topography is a principal requirement for the spatial-temporal analysis of temperature inhomogeneity in the bottom layer, no explicit scheme of AABW flow through the Doldrums, Vernadsky, and Pushcharovsky exists.

Therefore, using results of these previous works in conjunction with new data collected during the 33rd cruise of the R/V *Akademik Nikolaj Strakhov* (2016), this work aims to clarify the AABW pathways in the 7–8°N segment of the MAR using statistical analysis of the potential temperature distribution across the Doldrums, Vernadsky, and Pushcharovsky FZs taking into account the influence of bottom topography.

Materials and Methods

In order to track the spreading of AABW across the northern equatorial MAR, our approach consisted of a statistical analysis of the potential temperature field over three FZs: Pushcharovsky (7°28′ N), Vernadsky (7°43′ N), and Doldrums (8°14′ N). Potential temperature was derived from CTD profiling data which were analysed within the framework of new global bathymetric models [*GEBCO*, 2020; *Tozer et al.*, 2019] and additional original multibeam echosounder survey data (MBES).

Variational analysis (interpolation) was applied to the dataset using the Data-Interpolating Variational Analysis in n-dimensions (DIVAnd) software [*Barth et al.*, 2014]. DIVAnd is an open-source software written in Julia and widely used for data interpolation purposes. It can be used for in situ data analysis [*Dai et al.*, 2020], mapping of the climate atlases and calculation of the oceanographic databases [*Belgacem et al.*, 2021; *Korablev et al.*, 2014; *Troupin et al.*, 2010], and ocean currents research [*Barth et al.*, 2021].

Oceanographic data. The CTD dataset was compiled from data from the World Ocean Database (WOD18) [*Boyer et al.*, 2018] in the date range 2015–2018 with data collected during the scientific cruises of the Shirshov Institute of Oceanology, Russian Academy of Sciences (IO RAS). The IO RAS research cruise data included the 39th–41st cruises of the R/V *Akademik Sergey Vavilov* conducted in 2014–2016 [*Morozov et al.*, 2017] and from the 33rd cruise of the R/V *Akademik Nikolaj Strakhov* conducted in 2016 (Figure 2, Supplementary material). Overall, the analyzed dataset included 61 CTD profiles (Figure 3).

Oceanographic measurements during three research cruises on the R/V *Akademik Sergey Vavilov* in 2014–2016 were acquired using the CTD profiler Sea-Bird SBE 19plus SeaCAT [*Morozov et al.*, 2013, 2015, 2018]. The precision of the measurements was up to 0.005°C. The probe was calibrated in the Sea-Bird Electronics Laboratory, and additional intercalibration was carried out during two cruises with the high-precision reversing ther-

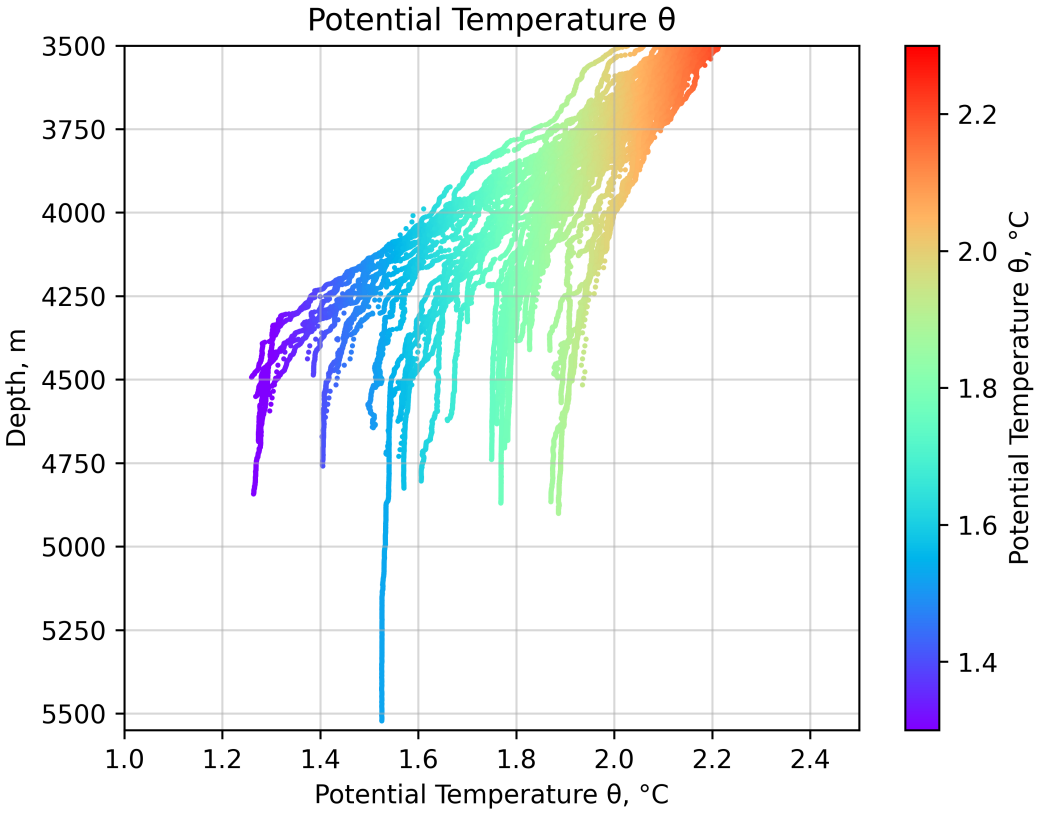

Figure 3. Scatterplot of the potential temperature values of the waters deeper than 3500 m at the 61 stations within 7–8°N segment of the MAR area.

mometer RTM 4002 X. The intercalibration results showed a mean difference between the probes of about 0.003°C.

The CTD profiles collected during the 33rd cruise of the R/V *Akademik Nikolaj Strakhov* (2016) were acquired using a Neil Brown Instrument Systems Mark III CTD profiler. The accuracy of the CTD profiler according to the specification is ∼ 0.005°C for the temperature sensor and 6.5 dbar for the pressure sensor. Calibration of the CTD profiler's sensors was performed at the Atlantic Branch of the IO RAS. Empirical coefficients and formulas for the profiler's measurements correction were derived. Corrected measurements had mean conductivity, temperature, and pressure uncertainties of about 0.005 mSm/cm, 0.005°C, and 8 dbar, respectively. Additionally, the data of the high-precision reversing thermometers SIS RTM 4002 and barometers SIS RPM 6000X were used to verify the results of DIVAnd analysis, though the data itself were not included in the analysis. The thermometers were accurate up to ∼0.003°C within the range between −2.0°C and 40°C. Barometers had an accuracy of about 0.1% of the water column pressure.

The depth and potential temperature were derived from the conductivity, temperature, and pressure measurements using the Thermodynamic Equation of SeaWater 2010 (TEOS-10). The equations are implemented in the Gibbs-SeaWater (GSW) Oceanographic Toolbox software [*McDougall and Barker,* 2011].

Bathymetry. During the 33rd cruise of the R/V *Akademik Nikolaj Strakhov* a bathymetric survey was carried out in the rift valleys of the Doldrums and Vernadsky FZs, the rift valley between them and areas of the Pushcharovsky FZ valley (see Figure 2). The survey's acquisition system consisted of the 12 kHz multibeam echosounder Reson 7150 for bathymetry data acquisition and the integrated positioning system Applanix POS MV, which included two GNSS antennas used for the position, and heading computation Trimble DSM132 and an inertial measurement unit used for attitude and heave measurements. Data acquisition and processing were done with PDS2000 v.3.7.0.47 software package. Water column speed of sound profiles used for correct-

ing bathymetric measurements were derived from the temperature and salinity profiles collected in the study area (Supplementary material, stations ANS-33043–33046). In accordance with the 6th edition of IHO Standards for Hydrographic Surveys (IHO Standards for Hydrographic Surveys, Edition 6.0.0, (2020), https://iho.int/en/standards-and-specifications, July, 2021), an analysis of both total vertical and total horizontal uncertainties (TVU and THU, respectively) was done to evaluate the quality of the collected data. Analysis of the initial data showed that for the given survey the average indicators of vertical and horizontal variability constituted ~ 55 and ~ 220 m, respectively, which corresponds well with the IHO Standards for Hydrographic Surveys for mean depths of 4150 m (IHO Standards for Hydrographic Surveys, Edition 6.0.0, (2020), https://iho.int/en/standards-and-specifications, July, 2021).

To perform a DIVAnd analysis, we required continuous and accurate (as much as possible) survey of seabed surface in the entire research area. The study area, at present, lacks sufficiently high-resolution bathymetric data and the multibeam survey carried out during the 33rd cruise of the R/V *Akademik Nikolaj Strakhov* was patchy. Therefore, two appropriate global DTMs were used: SRTM15+v2 [*Tozer et al.,* 2019] and GEBCO2020 [*GEBCO,* 2020] grids. Both have a 15 arcsecond resolution and both are essentially a combined product of single-beam, multibeam, and satellite-altimetry bathymetry. To define which DTM had the best representation of the seafloor in this area, we made two junctions of the MBES survey surface with SRTM15+v2 and GEBCO2020 surfaces. The junctions and their statistical analysis were made using QGIS software [*QGIS Development Team,* 2021] and Python [*van Rossum and Drake,* 1995] libraries – GDAL [*GDAL/OGR contributors,* 2021] and NumPy [*Harris et al.,* 2020]. The junction procedure included: median filtering of the MBES DTM to match the resolution of both global DTMs; surface difference derivation between the MBES and global DTMs; a simple statistical analysis of the difference surfaces – calculation of the mean and standard deviation of the difference surfaces; and creation of the histogram graph of the difference value distribution.

Multidimensional variational analysis DIVAnd. DIVAnd is a software tool for spatial interpolation (gridding) of oceanological parameters using in situ data [*Beckers et al.,* 2014]. DIVAnd is the implementation of the Variational Inverse Method (VIM), which resembles Optimal Interpolation (OI) methods (e.g., spline or kriging) [*Beckers et al.,* 2014; *Troupin et al.,* 2012]. DIVAnd has the following advantages:

- It is able to take into account boundaries (isobaths or coastlines), sub-basins, and various constraints (e.g., advection constraint).
- It was purposely designed for oceanographical in situ data analysis.
- It can provide quality control of the analysis field and estimate the used data quality [*Barth et al.,* 2014].
- DIVAnd is written in the modern programming language, Julia. It is easy to use and has a computationally effective gridding algorithm.

In the present work statistical analysis was performed on 55 horizons in the depth range of 3500–4600 m with vertical and horizontal resolutions of 20 m and 500 by 500 m, respectively. The analysis result was a regular three-dimensional (3D) grid for the 30 vertical layers (4000–4600 m) with a resolution of $500 \times 500 \times 20$ m.

Determination of the water mass boundaries. The benthic thermocline between AABW and Lower North Atlantic Deep Water (LNADW) vanishes when water passes through the MAR fractures thus, in the East Atlantic the boundary between AABW and LNADW becomes difficult to distinguish [*Mercier and Morin,* 1997]. The proportion of AABW in the bottom layer of the East Atlantic near the study area is estimated at 10–20% [*Johnson,* 2008].

Consequently, the position of the upper boundary of AABW in the East Atlantic can be determined as the boundary from [*Rhein et al.,* 1995, 1998] where a density anomaly of $\sigma_4 = 45.90$, which relates to temperatures of about 1.8°C, is assumed to be the boundary of the two water masses. This boundary is located at a depth of about 3900–4000 m at 7–8°N in the Guiana Basin west of the MAR. Besides, $\theta = 1.8$°C surface has been used as the AABW upper boundary in the western Atlantic in [*Friedrichs and Hall,* 1993; *Friedrichs et al.,* 1994; *Molinari et al.,* 1992]. In the East Atlantic, the $\theta = 2.0$°C isotherm at 11°N is accepted

Table 1: DIVAnd Analysis Parameters for Selected Layers

Parameter	Depth layer, m			
	4000	4200	4400	4600
Initially estimated correlation length, km	75.57	72.89	61.49	189.68
Initially estimated Epsilon2	0.08			
Optimized correlation length, km	429.18	917.63	774.17	91.99
Optimized Epsilon2	0.564	0.506	0.007	0.629
Weighting kernel size for closely spaced measurements, arcmins	$1.5' \times 1.5'$			
Estimation of the background field value of the potential temperature, °C	1.823	1.706	1.636	1.595

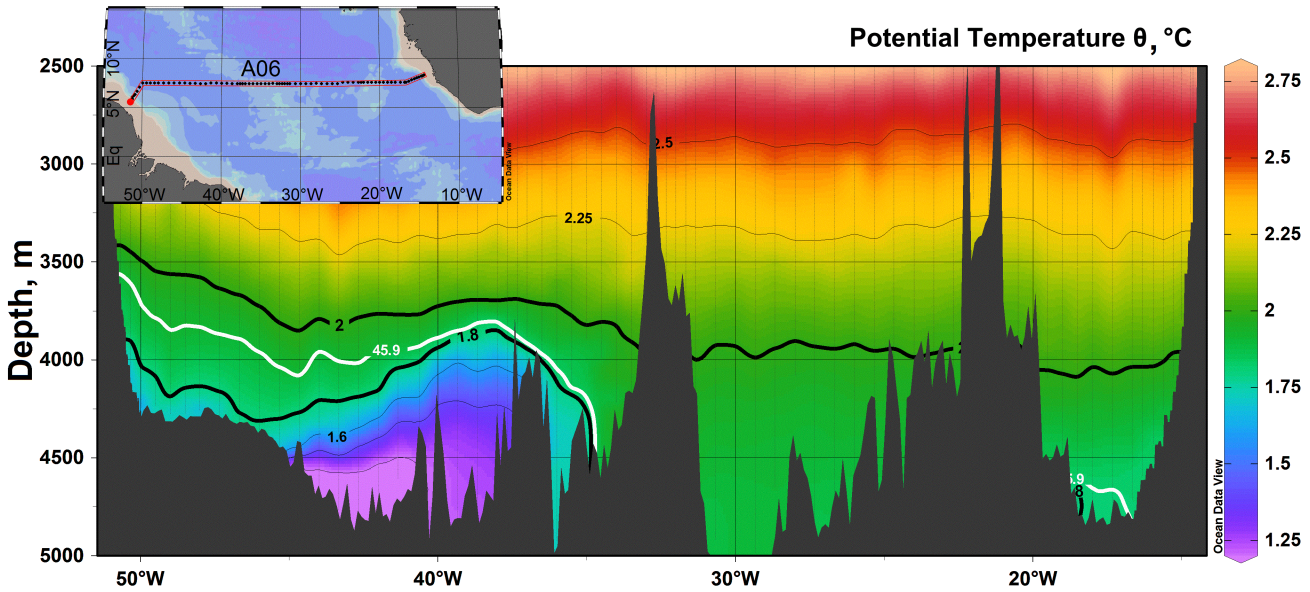

Figure 4. Potential temperature distribution over the WOCE A06 line at 7.5°N [*WOCE Hydrographic Programme,* 2002]. Isopycnic referenced to 4000 m (σ_4 = 45.90) and isotherms are shown. Inset – the WOCE A06 line location. Bathymetry from [*GEBCO,* 2020].

as the AABW upper boundary in Vema FZ [*McCartney et al.,* 1991].

In the study area, the potential density σ_4 = 45.90 and the 1.8°C isotherm are located shallower than in the Guiana Basin, according to the potential temperature distribution over the World Ocean Circulation Experiment (WOCE) A06 line at 7.5°N [*WOCE Hydrographic Programme,* 2002] (Figure 4).

DIVAnd Epsilon2 and L estimation. The key function of the DIVAnd tool is DIVAndrun, which requires the next inputs: in situ data represented by the anomalies of the analyzing parameter (value minus mean value of the potential temperature within a selected layer (background field value), Table 1), the analysis boundaries (mask), the correlation length parameter L, and the parameter Epsilon2, which is a qualitative estimation of the used dataset uncertainty. Epsilon2 and L parameters were defined based on potential temperature values and geographic position of the stations.

The initial parameter Epsilon2 is contextual and represents a qualitative assessment of the data and its uncertainty. The main factors influencing the uncertainty of the data within the study area are

temporal data irregularity and methodological error (different accuracy of the instruments used, difference in measurement techniques, etc.). We accepted the initial value of Epsilon2 as 0.08.

The initial correlation length parameter L was calculated using the DIVAnd_fitforhorlen function, which estimates the average correlation distance (in km) by determining the nature of the mutual influence of potential temperature measurements (i.e., the degree of their spatial coherence). This function does not consider the physical boundaries and analyzes only the dataset values and the initial parameter Epsilon2. Although it is an estimate, the initial parameter L obtained may approach reality if there are no boundaries between the measurements.

The DIVAnd_cv function optimized the primary parameters of Epsilon2 and L. The function is based on the cross-validation taking into account isobaths. As an illustration, the optimized Epsilon2 and L parameters for some of the analyzed layers are presented in Table 1. As it turned out, the initial and optimal Epsilon2 parameters differed on average by less than an order of magnitude, while the correlation length parameter L differed by slightly more than an order of magnitude. Such variations may be caused by the analyzed dataset's low spatial and temporal homogeneity within a particular depth layer and the complexity of the bottom topography.

The optimized Epsilon2 values of the closely spaced measurements were weighted to avoid the negative impact on the interpolation result. The weighting kernel size was 1.5×1.5 arcmins (~ 3 km^2). The background field value of potential temperature was defined for each layer to calculate potential temperature anomalies.

Quality Control. The analysis quality control (QC) was performed using the QC DIVAnd functions: DIVAnd_residualobs (residuals analysis), DIVAnd_qc (standard cross-validation), and DIVAnd_aexerr (almost exact error field associated with the analysis grid cells, further – error field). QC included: (a) calculation of the difference between the in situ measurements and the analysis results at the measurement stations (i.e., residuals derivation); (b) cross-validation of the data. Observations with a cross-validation value greater than 2 were considered "suspicious", i.e., poorly compatible with neighboring measurements. Such

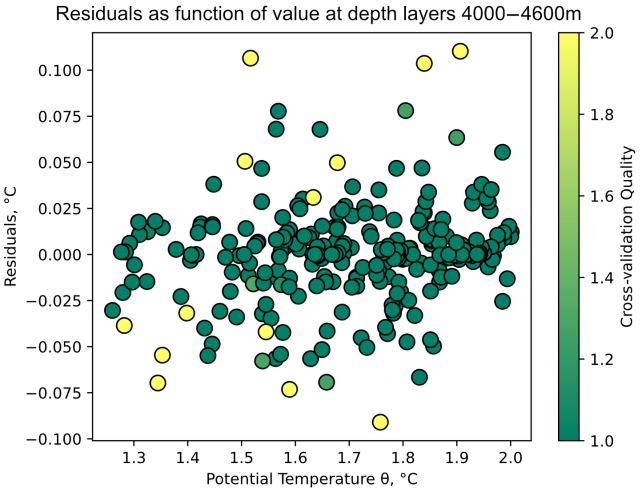

Figure 5. Scatterplot of residuals as a function of potential temperature. The dot color corresponds to the unitless observation quality value derived by cross-validation. In 6 layers (4000–4600 m in 100 m) there are 294 potential temperature values. Observations with a depth more than the DTM's depth were not included in the analysis and not shown on the graph.

inconsistencies could be a consequence of either a methodological error in the observations or inaccuracy of the seabed topography or a result of hydrodynamic processes at the area of the "suspicious" measurement (e.g., temporal variability of oceanological characteristics); (c) variational analysis of the randomly located measurements and calculating the error field.

Based on (a) and (b) QC steps, we created a scatterplot of the residuals as a function of the potential temperature observations for 6 depth layers within the 4000–4600 m range with 100 m step (Figure 5). The average residual values were no more than ± 0.05°C. Observations with residual values above the 0.05°C confidence intervals were considered suspicious. Possible causes included: inconsistency between the observations and neighboring measurements or poor optimization of the parameters Epsilon2 and L for the observations.

The QC of the potential temperature data and performed analysis was assumed to be successful – (a) and (b) steps, and scatterplot analysis did not reveal any significant issues with the chosen Epsilon2 and L parameters and the used dataset. Hence, the optimized parameters Epsilon2 and L and the observations dataset were deemed appropriate and the performed DIVAnd analysis of the 55th depth layers within the range of 3500–

Table 2: The Filtering Statistics

Grids	Grid cells			
	Number of non-empty cells, thousands	%-age of the cells of the initial number	Number of the rejected cells, thousands	%-age of the rejected cells of the initial number
Initial (unfiltered) DIVAnd analysis grid	5173 (initial)	100% (78.41%)	0	0%
Filter-A grid	2268	43.84%	2905	56.15%
Filter-B grid	1686	32.56%	582	11.25%
Overall filtering stats	1686	32.56%	3487	67.40%

4600 m was considered acceptable. This depth range exceeded the investigated depth range (4000–4600 m), intending to remove the possible vertical inconsistency. The error field calculated in step (c) could be used if the analysis parameters, dataset, and therefore performed analysis are deemed acceptable. The error field grid had the same dimensions and resolution as the analysis grid and characterized the analysis uncertainty.

Filtering. As the final step filtration of the results of the analysis consisted of the removal of grid cells values that had a vertical inconsistency (the temperatures of the overlying cells were colder than the underlying ones (Filter-A)) and removal of those cell values for which the error field value exceeded 0.05°C and more (Filter-B). The filtering statistics are shown in Table 2.

Bottom temperature analysis. As a secondary product of the multidimensional analysis, we calculated the two-dimensional (2D) grid of the bottom potential temperature distribution using the same DIVAnd gridding algorithm. A new dataset for 2D analysis was computed by sampling the 3D grid's potential temperature values. The sampling criteria were: (a) cell values of the 3D grid should have a depth that differs by no more than 300 m from the DTM's depth; (b) this value should belong to the deepest cell of cell values selected according to the rule (a). The depth source was presented by the same combined DTM as for 3D analysis. The Epsilon2 and Correlation Length L parameters used were 0.8 and 100 km, respectively.

Results and Discussion

Combined DTM. The result of the MBES survey performed in 2016 by R/V *Akademik Nikolaj Strakhov* was a DTM of the seabed of 100×100 m spatial resolution covering Doldrums, Pushcharovsky, and Vernadsky FZs (Figure 6).

The junctions performed between MBES DTM and two global DTMs – SRTM15+v2 [*Tozer et al.*, 2019] and GEBCO2020 [*GEBCO*, 2020] resided by analyzing two grids of the depth value differences: (1) between MBES DTM and SRTM15+V2 grids; (2) between MBES DTM and GEBCO2020 grids (Figure 7) showed us next: (a) the mean depth difference for case (1) was 36% less than (2); (b) the standard deviation of the depth difference values distribution for case (1) was 21.5% less than (2). Both (a) and (b) revealed explicit evidence that SRTM15+V2 DTM is more representative of the seabed within the research area compared to GEBCO2020. So, in combination with MBES DTM, SRTM15+V2 provided the most accurate seabed surface representation available.

Flows of AABW in the fracture zones of the MAR. At some stations the values of potential temperature were deemed "suspicious" by the DIVAnd analysis (Figure 8). Most of the "suspicious" values are related to the difference in the

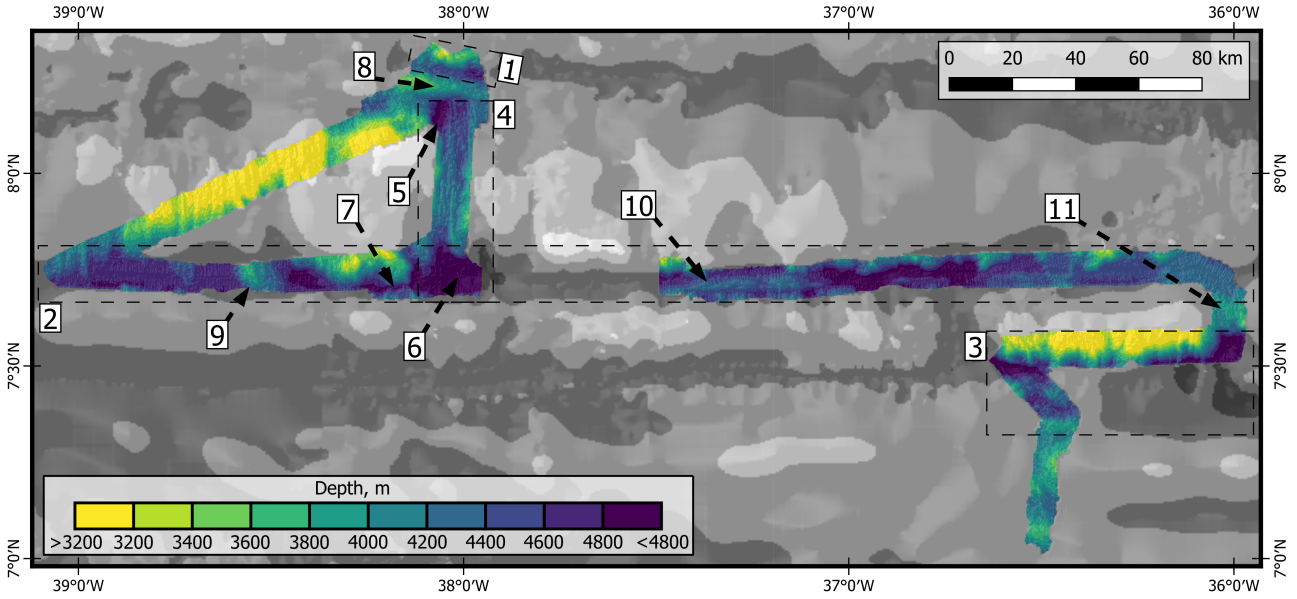

Figure 6. The DTM based upon the bathymetric survey of the 33rd cruise R/V *Akademik Nikolaj Strakhov* overlayed on the SRTM15+v2 grid [*Tozer et al.*, 2019]. Digits define the following seabed features: (1) Doldrums FZ; (2) Vernadsky FZ; (3) Pushcharovsky FZ; (4) rift valley between Doldrums and Vernadsky FZs; (5, 6) nodal depressions; (7) deep gap in the western part of the Vernadsky FZ; (8) the median ridge between the rift valley and Doldrums FZ; sills in western (9) and central (10) parts of the Vernadsky FZ, and (11) wide sill between Vernadsky and Pushcharovsky FZs.

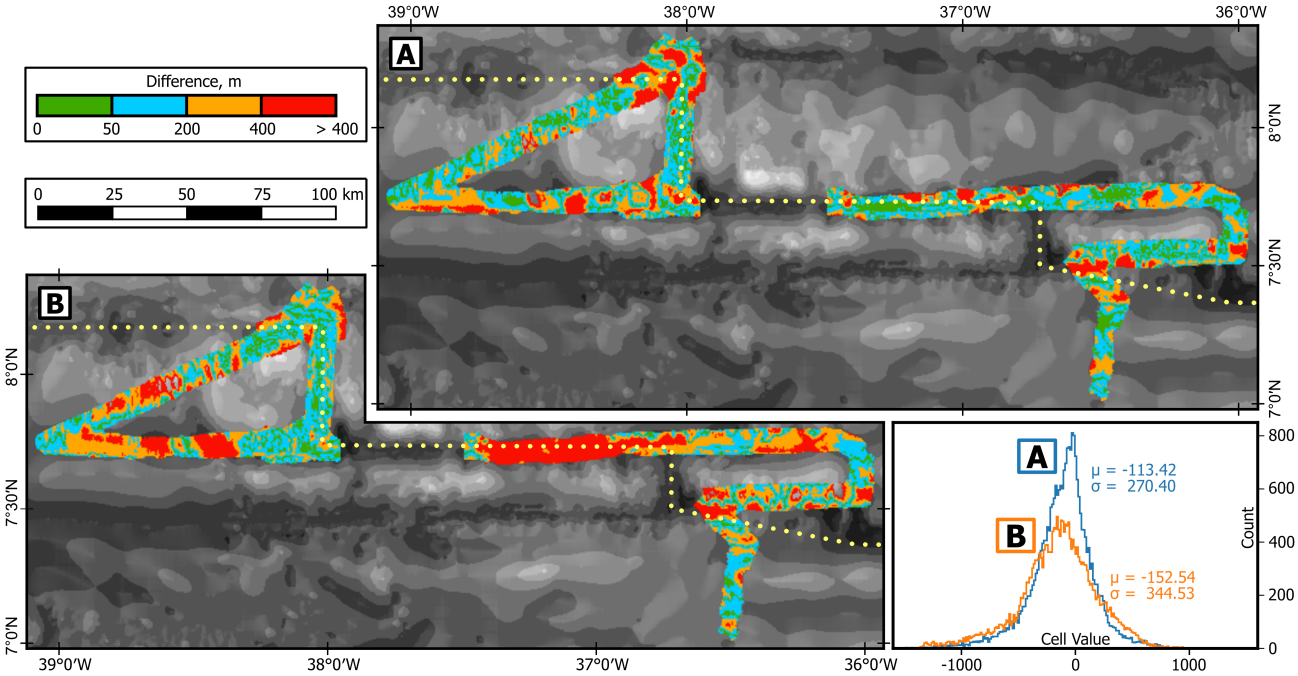

Figure 7. Grids of the differences between MBES DTM from the 33rd cruise of the R/V *Akademik Nikolaj Strakhov* bathymetric data and the global DTMs (A) SRTM15+V2 [*Tozer et al.*, 2019] and (B) GEBCO2020 [*GEBCO*, 2020], and histograms of the depth difference values distributions.

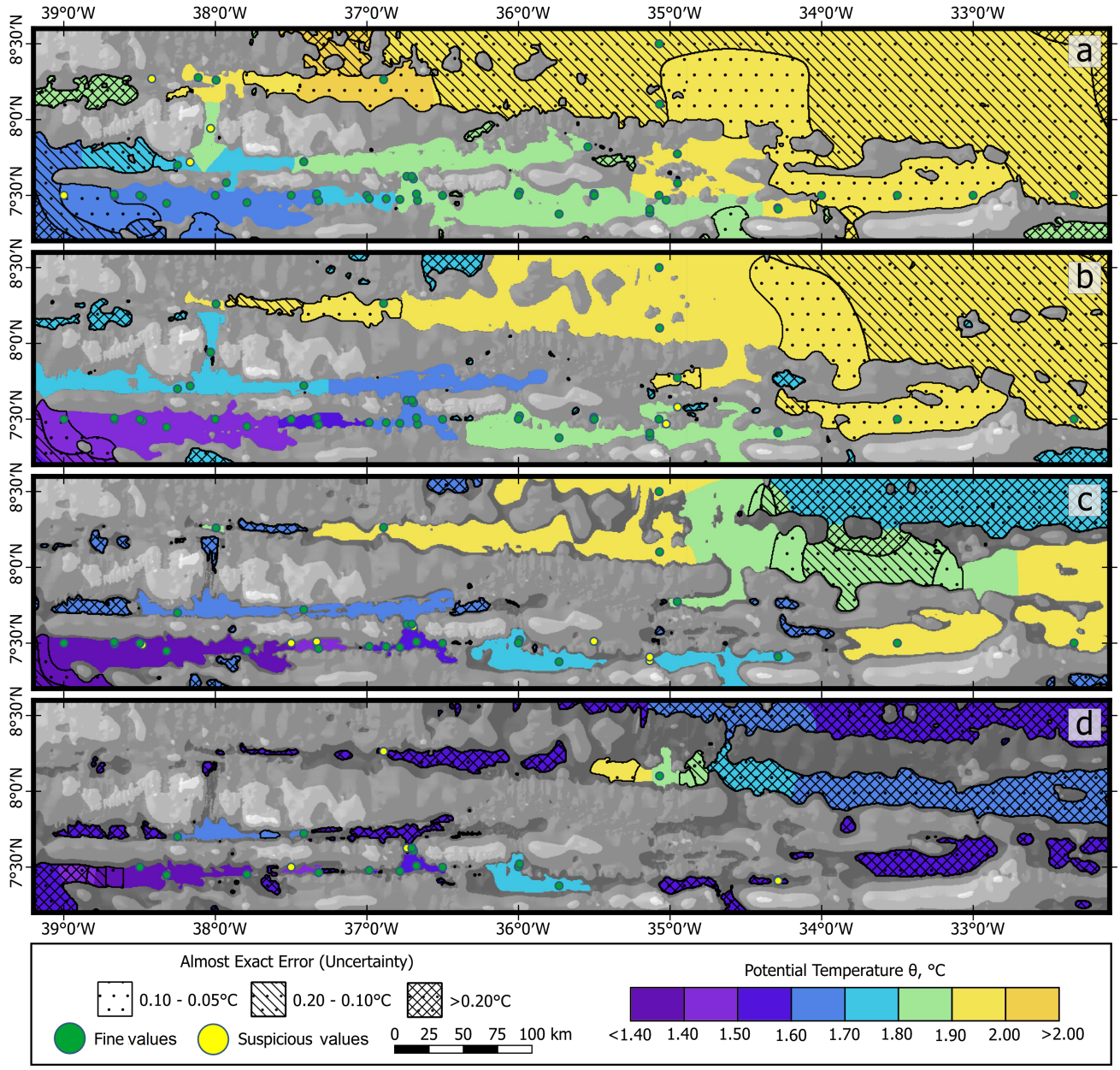

Figure 8. Potential temperature distribution in Doldrums, Vernadsky, and Pushcharovsky FZs for (a) 4000 m, (b) 4200 m, (c) 4400 m, and (d) 4600 m layers. Areas of varying uncertainty of analysis results (error field) are shown by hatching. Yellow-marked measurements have been labeled as "suspicious".

potential temperature values at the closely located stations. For the "suspicious" values associated with the sills and narrow passages of fracture zones these differences could be explained by the complex hydrological conditions in these bathymetric features. Besides, such differences may be associated with temporal variability in the temperature associated with tidal currents [*Morozov,* 1995; *Morozov et al.,* 2008]. For example, it is known that in the neighboring Vema FZ, the variability of the potential temperature at the 4000-m isobath was found to be 0.06°C [*Demidov et al.,* 2007], while the diurnal variability of the AABW temperature [*Demidov et al.,* 2020] reached 0.05°C. The position of the 1.45 and 2.00°C isotherms in the Vema FZ could vary daily within 0–300 m and 0–200 m, re-

spectively. This fact suggests that a similar pattern of variability may be observed in the neighboring fracture zones.

A few "suspicious" values are related to the fact that the depth of the measurement used in the analysis is greater than the DTM depth at this station, which is due to the lack of accuracy of the bathymetric data making it impossible to analyze these measurements.

Figure 8 shows the potential temperature distribution in several layers based on the results of the analysis. The uncertainty of potential temperature analysis increases in areas poorly supported by initial data. In addition, the analysis uncertainty increases where physical (isobath) boundaries are lacking.

The largest uncertainty is found in the northeast of the study area for the depth of 4600 m. This relates to the absence of the temperature measurements. Nevertheless, the initial data and the values of the parameters Epsilon2 and L allowed us to perform an analysis characterized by a sufficiently high degree of spatial consistency of the grid cell values with each other and with the surrounding relief. Filtering of the analysis results allowed us to eliminate both horizontal and vertical inconsistencies in the values of the 3D grid.

The results of the 2D analysis of the potential temperature distribution, taking into account bathymetry (Figure 9a), made it possible to develop a scheme of AABW propagation below 4000 m (Figure 9b). The minimal values of the potential temperature obtained at the oceanographic stations were also taken into consideration. The propagation scheme was made for "unmodified" AABW with a potential temperature up to 1.8°C [*Rhein et al.,* 1995, 1998], and "modified" AABW with a temperature of 1.8–2.0°C.

In the western part of the Pushcharovsky FZ, the minimum values of potential temperature within the bottom layer ($\theta < 1.4$°C) were recorded at depths exceeding 4250 m. Sill 1 (Figure 9a, 37.08°W, depth 4290 m) prevents the penetration of the coldest water further eastward. At the same time, some fraction of the AABW flows into the Vernadsky FZ to the north over sill 2 (37.88°W, 4130 m). Both eastward of sill 1 and northward of sill 2, AABW in the bottom layer becomes slightly warmer, 1.5–1.6°C and 1.6–1.7°C, respectively.

After flowing over sill 1, the majority of AABW in the Pushcharovsky FZ spreads over sill 3 (36.73°W, 4580 m) and propagates into the Vernadsky FZ. A minor fraction of AABW propagates into the East Atlantic along the Pushcharovsky FZ and passes through sill 4 (4030 m), where it is likely that the flow splits into two branches: part of the flow goes eastward over sill 5 (4200 m), and another part spreads northward, towards the shallow sills 6–8 (4060–4160 m). In the eastern part of the FZ, the AABW reaches sill 9 (34°W, 4010 m). Antarctic waters with potential temperature less than 1.8°C cannot propagate past this sill.

As previously mentioned, a slightly colder AABW enters the Vernadsky FZ via sill 3 compared to sill 2 (Figure 9a). This water has a temperature of 1.5–1.6°C. Along the Vernadsky FZ itself, AABW with a temperature of 1.6–1.7°C enters from the west through sills 10 (38.53°W, 4360 m) and 11 (38.3°W, 4530 m). With such a combination of sources after sill 3, AABW not only continues moving eastward to 35.53°W, but also turns backward – westward, crossing sills 12–14 with depths up to 4410–4450 m. This multi-source AABW fills the basin below 6000 m deep. The temperature here is about 1.6–1.7°C.

From the area of the nodal depression, the AABW spreads northward (over sill 15) to the rift valley between the Doldrums and Vernadsky FZs where it most likely turns to flow along the north walls of the rift valley and the shallow sill 16 (4110 m), returning back to the area of the nodal depression. The absence of the densest water flow over the sill is reflected in the potential temperature measured over sill 16 (1.96°C) and beyond this sill (1.89°C), with temperatures within the rift valley reaching 1.8°C). The overflow across the sill between the rift valley and the Doldrums FZ (sill 16 in Figure 9a) is likely accompanied by a strong bottom current, so-called the underwater cataract [*Whitehead,* 1998]. Similar cataracts are described in [*Morozov et al.,* 2012; *Whitehead,* 1998]. "Modified" AABW with a temperature greater than 1.8°C, crossing this sill, flows eastward to 38.2°W and westward over sill 17 (4170 m), along the Doldrums FZ. After flowing over sills 16 and 17, "modified" AABW flows further eastward along the Doldrums FZ into the East Atlantic (Figure 9b).

In the western part of the Doldrums FZ, there is a wide sill at a depth of approximately 3800 m.

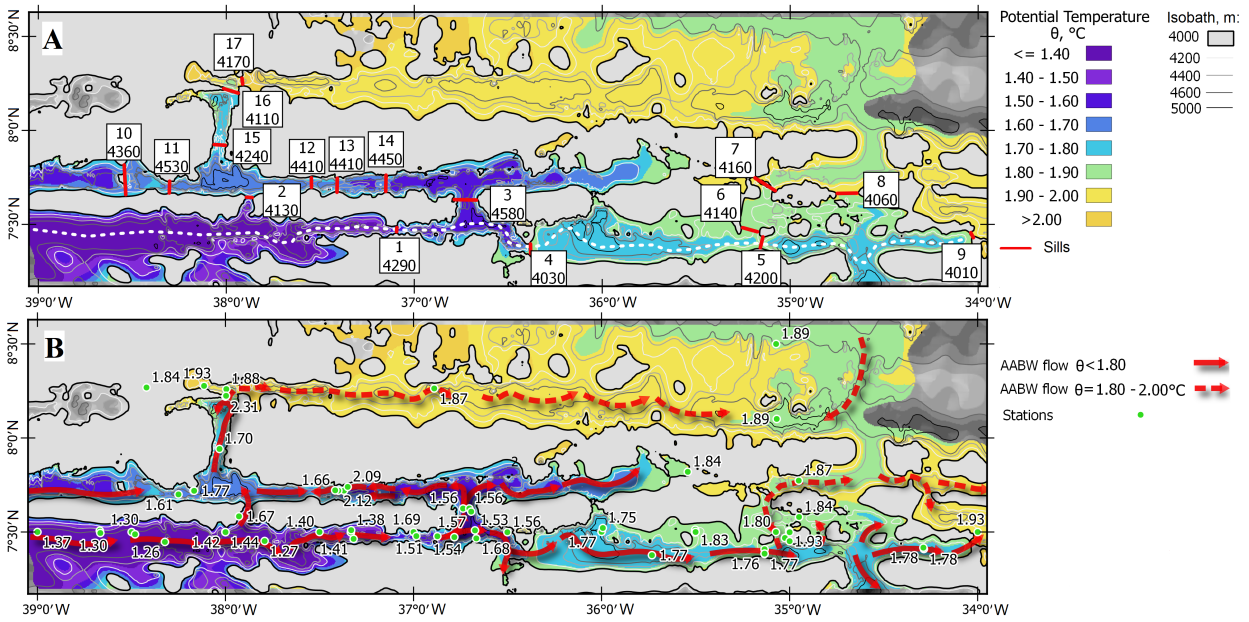

Figure 9. Distribution of the bottom potential temperature in the Doldrums, Vernadsky, and Pushcharovsky FZs. a – DIVAnd analysis results, the main sills with its numbers and depths. The white dotted line shows the location of the oceanographic section; b – DIVAnd analysis results, stations with the minimum potential temperature at the bottom and AABW spreading scheme (solid arrows – water with a potential temperature of less than 1.8°C, dotted lines – with a temperature of 1.8–2°C). Isobaths – every 200 m.

This sill may block AABW in its westward migration. It is likely that water with temperatures less than 1.85–1.9°C does not leave the Doldrums FZ. It is also possible that water in the eastern part of the Doldrums FZ mixes with AABW coming both from the Pushcharovsky FZ and from the Vema FZ. This is indirectly indicated by the presence of the shallow sills 7 and 8 with depths of 4060–4160 m. Those sills may prevent the spread of water with temperatures below 1.9°C, and changes in the 1.9°C isobath depth over the section along the Pushcharovsky FZ east of 35°W (Figure 10). This may be associated with both the flow of AABW from the Vema FZ and with tidal processes [*Morozov,* 1995; *Demidov et al.,* 2020].

The presented analysis suggests that water with a potential temperature of 1.8–2.0°C flows into the East Atlantic from the studied fracture zones. The DTM shows that to the south and to the south of this area, there are sills with depths of less than 3800 m, which prevent the flow of AABW eastward (Figure 9). To the north of studied fractures, water with a potential temperature of 1.85°C was recorded at a depth of 3955 m in the Arkhangelsky FZ to the west of the 3700-m sill [*Morozov et al.,* 2017]. That indicates no overflow of AABW with a temperature less than 1.8°C to the East Atlantic.

Conclusions

The Data-Interpolating Variational Analysis in n-dimensions statistical analysis of the potential temperature distribution was based on the original DTM obtained by supplementing the STRM15+ DTM with data from the 33rd cruise of the R/V *Akademik Nikolaj Strakhov*. CTD data from the WOD18 [*Boyer et al.,* 2018] from 1995, supplemented with data from IO RAS cruises (39th–41st cruises of the R/V *Akademik Sergey Vavilov* in 2014–2016 and the 33rd cruise of the R/V *Akademik Nikolaj Strakhov* (in 2016) were used as initial temperature data. A total of 61 oceanographic stations were included in the analysis.

The result of the potential temperature distribution analysis carried out with DIVAnd was a three-dimensional grid of the potential temperature with a spatial resolution of 500 × 500 × 20 m. The analysis QC allowed us to quantify the uncertainty in each individual grid cell. Filtering of grid cells on the basis of these QC allowed us to completely eliminate the areas of spatial inconsistency in the analysis and thus provide an objective model of potential temperature field distribution in the region of the Mid-Atlantic Ridge fractures at 7–8°N.

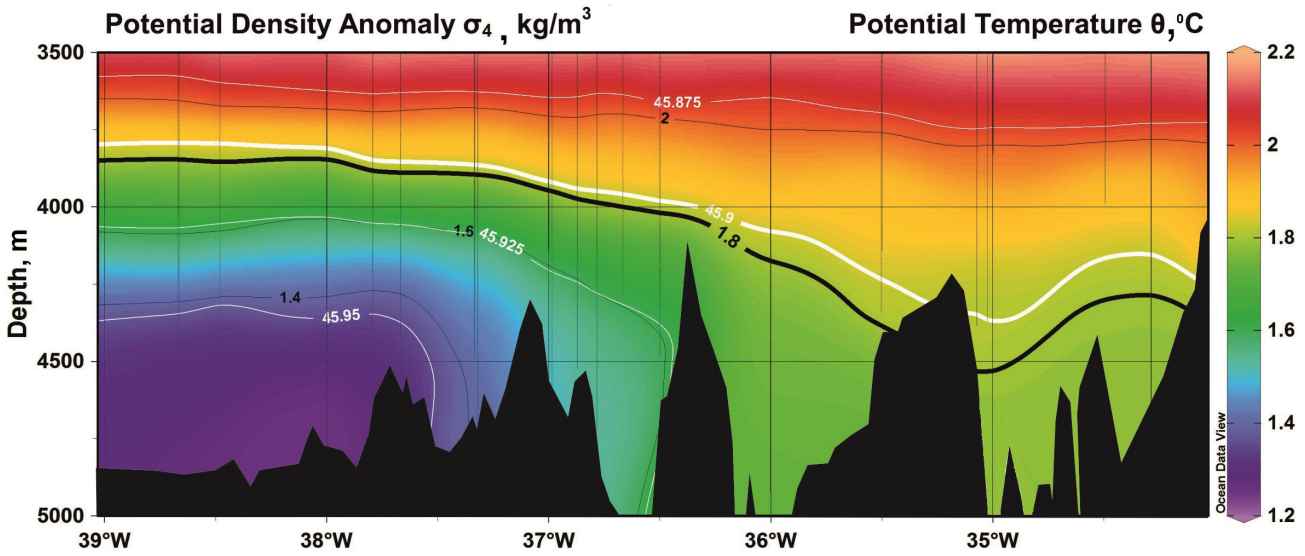

Figure 10. Potential temperature distribution over the section in Pushcharovsky FZ. Isopycnic referenced to 4000 m (white lines) and isotherms (black lines) are shown.

Based on the DIVAnd analysis, a 2D model of near-bottom potential temperature distribution in the study area was calculated. This model allows us to propose the pattern of AABW propagation through the Doldrums, Vernadsky, and Pushcharovsky FZs. The main flow of "unmodified" AABW (with potential temperature less than 1.8°C) in these fractures propagates through the Pushcharovsky FZ. Part of the water, overcoming sills up to 4030 m deep, warming up to 1.8°C, propagates eastward along this FZ to 34°W; part of the AABW penetrates into the Vernadsky FZ through transverse sills 2 and 3, where it mixes with the AABW coming into this FZ from the west. Then, AABW from different sources spreads northward along the rift valley (up to 5300 m deep) to the sills 16 and 17. Through these sills, only "modified" AABW spreads eastward and in the eastern part of the Doldrums FZ probably mixes with water outflowing from the Vema FZ and from the Pushcharovsky FZ.

Taking into consideration the bathymetry improves our understanding of the flow of AABW in Doldrums, Vernadsky, and Pushcharovsky FZs. AABW warms up when passing fracture zones from 1.4°C in Pushcharovsky FZ up to 1.9–2.0°C in Doldrums FZ. There is no overflow of AABW with a potential temperature less than 1.8°C to the East Atlantic in this area.

Acknowledgments. The expedition and the primary processing of the data obtained during the 33rd cruise of the R/V *Akademik Nikolaj Strakhov* (2016) were supported by the state assignment of IO RAS, no. FMWE-2021-0012. The analysis and interpretation of the data were funded by the project of the Russian Science Foundation no. 19-17-00246. The data obtained during cruises 39th–41st of the R/V *Akademik Sergey Vavilov* were analyzed within the framework of the project of the Russian Foundation for Basic Research no. 20-08-00246. The authors are grateful to Prof. E. G. Morozov (IO RAS) for providing oceanographic data obtained during the 39th–41st cruises of the R/V *Akademik Sergey Vavilov* and to Prof. S. A. Dobrolyubov (Lomonosov Moscow State University) for providing thermometers for the 33rd cruise of the R/V *Akademik Nikolaj Strakhov*. The authors also express their gratitude to the participants of the 33rd cruise of the R/V *Akademik Nikolaj Strakhov*: I. A. Mironov (Lomonosov Moscow State University), V. M. Pyatakov, and A. B. Demenina (IO RAS) for their help in collecting of oceanographic and bathymetric data and the crew of the R/V for their assistance in carrying out the scientific work. The authors are grateful to Dr. D. V. Dorokhov (IO RAS) for fruitful discussion and valuable recommendations and to T. Glazkova (Royal Holloway, University of London) for English corrections.

Appendix A

Supplementary material

CTD-profiling and thermometers stations used in the study.
Underlined are the depth (DTM) that do not exceed the measurement horizon.

No.	Station	Latitude, °N	Longitude, °W	Date	Potential temperature, °C	Instrument depth, m	Bottom depth (DTM), m
1	ANS-33043	07° 43.15'	38° 10.00'	Nov. 30, 2016	1.775	4235	4391
2	ANS-33044	08° 13.45'	37° 59.81'	Dec. 1, 2016	1.806	3954	4048
3	ANS-33045	08° 16.62'	38° 06.83'	Dec. 1, 2016	1.927	4129	4333
4	ANS-33046	08° 15.60'	37° 59.73'	Dec. 1, 2016	1.885	4495	4648
5	ASV-2556	07° 56.50'	38° 01.90'	Oct. 10, 2014	1.700	4327	4298
6	ASV-2557	07° 43.30'	37° 25.00'	Oct. 11, 2014	1.660	4623	4647
7	ASV-2558	07° 28.70'	36° 59.10'	Oct. 11, 2014	1.508	4644	4666
8	ASV-2573	08° 15.80'	36° 53.40'	Sept. 23, 2015	1.871	4866	4502
9	ASV-2574	07° 36.50'	36° 41.60'	Sept. 23, 2015	1.571	4825	4745
10	ASV-2575	07° 49.20'	35° 32.50'	Sept. 24, 2015	1.835	4073	4113
11	ASV-2576	07° 23.10'	35°08.00'	Sept. 24, 2015	1.758	4524	4216
12	ASV-2597	07° 23.00'	35° 08.00'	Apr. 19, 2016	1.765	4526	4180
13	ASV-2598	07° 24.50'	35° 08.00'	Apr. 19, 2016	1.765	4424	4233
14	ASV-2599	07° 28.10'	35° 01.50'	Apr. 19, 2016	1.799	4370	4106
15	ASV-2600	07° 34.80'	34° 57.00'	Apr. 20, 2016	1.839	4216	4088
16	ASV-2601	07° 46.40'	34° 57.10'	Apr. 20, 2016	1.869	4413	4420
17	ASV-2602	07° 37.50'	36° 44.20'	Apr. 21, 2016	1.564	4619	4578
18	ASV-2603	07° 37.50'	36° 42.20'	Apr. 21, 2016	1.558	4625	4595
19	ASV-2604	07° 42.00'	38° 15.00'	Apr. 21, 2016	1.606	4804	4885
20	ASV-2655	08° 16.10'	38° 25.20'	Oct. 23, 2016	1.836	4034	3655
21	ASV-2658	07° 35.00'	37° 55.70'	Oct. 24, 2016	1.671	4081	4065
22	WOD-3351448	07° 29.28'	38° 28.86'	Aug. 20, 1983	1.260	4493	4760
23	WOD-7744331	07° 27.07'	35° 00.00'	Feb. 22, 1993	1.956	3888	3963
24	WOD-7909476	07° 29.95'	38° 00.03'	Sept. 17, 1995	1.436	4381	4434
25	WOD-7909478	07° 27.96'	36° 39.97'	Sept. 18, 1995	1.678	4292	4344
26	WOD-7909480	07° 29.85'	35° 30.20'	Sept. 19, 1995	1.829	4342	4208
27	WOD-7909481	07° 29.93'	35° 00.00'	Sept. 19, 1995	1.943	3825	3941
28	WOD-7909565	07° 29.96'	37° 59.99'	Apr. 24, 1996	1.379	4358	4434
29	WOD-7909570	07° 30.72'	35° 30.12'	Apr. 25, 1996	1.827	4411	4213
30	WOD-7909571	07° 30.32'	35° 00.14'	Apr. 26, 1996	1.932	3816	4012
31	WOD-8078420	07° 29.68'	38° 39.93'	Sept. 17, 1995	1.297	4545	4591
32	WOD-8078423	07° 29.86'	37° 20.00'	Sept. 18, 1995	1.428	4473	4575
33	WOD-8078426	07° 30.13'	36° 00.03'	Sept. 18, 1995	1.761	4633	4706
34	WOD-8078643	07° 30.43'	38° 40.10'	Apr. 24, 1996	1.268	4551	4467
35	WOD-8078644	07° 30.58'	37° 19.89'	Apr. 24, 1996	1.386	4487	4706
36	WOD-8078645	07° 30.52'	36° 40.39'	Apr. 25, 1996	1.525	5522	5085
37	WOD-8078646	07° 31.29'	35° 59.60'	Apr. 25, 1996	1.750	4740	4865

(Continuation of Supplementary material) CTD-profiling and thermometers stations used in the study. Underlined are the depth (DTM) that do not exceed the measurement horizon.

No.	Station	Latitude, °N	Longitude, °W	Date	Potential temperature, °C	Instrument depth, m	Bottom depth (DTM), m
38	WOD-11957615	07° 30.00’	35° 04.38’	Dec. 7, 2000	1.801	4384	4392
39	WOD-11957616	08° 06.07’	35° 04.12’	Dec. 7, 2000	1.886	4901	5058
40	WOD-11957617	08° 29.99’	35° 04.32’	Dec. 7, 2000	1.892	4569	4576
41	WOD-11957624	07° 22.61’	35° 43.93’	Dec. 10, 2000	1.768	4870	4804
42	WOD-11957726	07° 26.84’	38° 19.32’	June 14, 2002	1.264	4843	4905
43	WOD-11957727	07° 27.13’	37° 47.51’	June 14, 2002	1.274	4686	4737
44	WOD-11957728	07° 27.81’	37° 19.13’	June 15, 2002	1.405	4759	4572
45	WOD-11957729	07° 28.64’	36° 52.39’	June 15, 2002	1.513	4524	4536
46	WOD-11957731	07° 25.02’	34° 17.33’	June 16, 2002	1.783	4682	4508
47	WOD-11957919	07° 24.58’	34° 17.17’	June 1, 2003	1.776	4705	4562
48	WOD-11957920	07° 28.36’	06° 46.98’	June 2, 2003	1.536	4724	4800
49	WOD-13096323	07° 30.00’	39° 00.00’	Apr. 30, 2010	1.374	4438	4743
50	WOD-13096332	07° 30.00’	38° 29.90’	Apr. 30, 2010	1.297	4594	4683
51	WOD-13096341	07° 30.00’	38° 00.06’	Apr. 30, 2010	1.424	4340	4434
52	WOD-13096354	07° 30.00’	37° 30.00’	May 1, 2010	1.403	4671	4386
53	WOD-13096367	07° 30.00’	37° 00.00’	May 1, 2010	1.692	4126	4103
54	WOD-13096377	07° 29.94’	36° 30.06’	May 1, 2010	1.560	4730	4678
55	WOD-13096388	07° 30.06’	36° 00.00’	May 2, 2010	1.766	4555	4705
56	WOD-13096397	07° 30.00’	35° 30.00’	May 2, 2010	1.826	4301	4219
57	WOD-13096444	07° 30.00’	34° 00.00’	May 3, 2010	1.929	4594	4176
58	WOD-13096458	07° 30.00’	33° 30.00’	May 3, 2010	1.918	4418	5186
59	WOD-13096474	07° 30.00’	33° 00.00’	May 3, 2010	1.966	4184	4740
60	WOD-13096496	07° 30.06’	32° 20.04’	May 4, 2010	1.935	4516	4404
61	WOD-19080078	07° 29.92’	35° 00.07’	May 12, 2015	1.872	3853	3968
62	ANS-33040 (T)	07° 43.20’	37° 22.20’	Nov. 28, 2016	1.74	4376	4356
63	ANS-33041 (T)	07° 43.20’	37° 24.00’	Nov. 29, 2016	1.73	4617	4550
64	ANS-33042 (T)	07° 44.40’	37° 21.00’	Nov. 29, 2016	1.68	4572	4616
65	ANS-33043 (T)	07° 43.20’	38° 10.20’	Nov. 30, 2016	1.71	4282	4391
66	ANS-33044 (T)	08° 13.20’	38° 00.00’	Dec. 1, 2016	1.96	3937	4016

References

Barth, A., J. M. Beckers, et al. (2014), Divand-1.0: n-dimensional variational data analysis for ocean observations, *Geoscientific Model Development*, *7,* No. 1, 225–241, **Crossref**

Barth, A., C. Troupin, et al. (2021), Variational interpolation of high-frequency radar surface currents using DIVAnd, *Ocean Dynamics*, *71,* No. 3, 293–308, **Crossref**

Beckers, J. M., A. Barth, et al. (2014), Approximate and efficient methods to assess error fields in spatial gridding with data interpolating variational analysis (DIVA), *Journal of Atmospheric and Oceanic Technology*, *31,* No. 2, 515–530, **Crossref**

Belgacem, M., K. Schroeder, et al. (2021), Climatological distribution of dissolved inorganic nutrients in the Western Mediterranean Sea (1981–2017), *Earth System Science Data Discussions*, 1–49, **Crossref**

Boyer, T. P., O. K. Baranova, et al. (2018), *World Ocean Database 2018*, 207 pp. NOAA, NESDIS.

Dai, J., H. Wang, et al. (2020), Observed spatiotemporal variation of three-dimensional structure and heat/salt transport of anticyclonic mesoscale eddy in Northwest Pacific, *Journal of Oceanology and Limnology*, 1–22, **Crossref**

Demidov, A. N., S. A. Dobrolyubov, et al. (2007), Transport of bottom waters through the Vema Fracture Zone in the Mid-Atlantic Ridge, *Doklady Earth Sciences*, *416,* No. 7, 1120–1124, **Crossref**

Demidov, A. N., A. A. Ivanov, et al. (2020), Transport of deep and bottom waters through the Mid-Atlantic Ridge in the Vema fracture zone, *Doklady Earth Sciences*, *494,* No. 1, 735–740, **Crossref**

Demidov, A. N., E. G. Morozov, R. Y. Tarakanov (2011), Structure and transport of bottom waters through the chain fracture zone of the Mid-Atlantic Ridge, *Russian Meteorology and Hydrology*, *36,* No. 8, 542–548.

Frey, D. I., E. G. Morozov, et al. (2019), Regional modeling of Antarctic Bottom Water flows in the key passages of the Atlantic, *Journal of Geophysical Research: Oceans*, *124,* No. 11, 8414, **Crossref**

Friedrichs, M. A., M. M. Hall (1993), Deep circulation in the tropical North Atlantic, *Journal of Marine Research*, *51,* No. 4, 697–736, **Crossref**

Friedrichs, M. A., M. S. McCartney, M. M. Hall (1994), Hemispheric asymmetry of deep water transport modes in the western Atlantic, *Journal of Geophysical Research: Oceans*, *99,* No. C12, 25,165–25,179, **Crossref**

GDAL/OGR contributors (2021), *GDAL/OGR Geospatial Data Abstraction Software Library*, Open Source Geospatial Found., URL https://gdal.org.

GEBCO Bathymetric Compilation Group (2020), *The GEBCO_2020 Grid – a continuous terrain model of the global oceans and land*, British Oceanographic Data Centre, National Oceanography Centre, NERC, UK.

Harris, C. R., K. J. Millman, et al. (2020), Array programming with NumPy, *Nature*, *585,* No. 7825, 357–362, **Crossref**

Johnson, G. C. (2008), Quantifying Antarctic bottom water and North Atlantic deep water volumes, *Journal of Geophysical Research: Oceans*, *113,* C5, **Crossref**

Korablev, A., O. K. Baranova, et al. (2014), Climatological atlas of the Nordic Seas and northern North Atlantic, *NOAA Atlas NESDIS*, *77,* 122.

Locarnini, R. A., T. Whitworth, W. D. Nowlin (1993), The importance of the Scotia Sea on the outflow of Weddell Sea Deep Water, *Journal of Marine Research*, *51,* No. 1, 135–153, **Crossref**

McCartney, M. S., S. L. Bennett, et al. (1991), Eastward flow through the Mid-Atlantic Ridge at 11 N and its influence on the abyss of the eastern basin, *Journal of Physical Oceanography*, *21,* No. 8, 1089–1121, **Crossref**

McDougall, T. J., P. M. Barker (2011), Getting started with TEOS-10 and the Gibbs Seawater (GSW) oceanographic toolbox, *SCOR/IAPSO WG*, *127,* 1–28.

Mercier, H., K. G. Speer (1998), Transport of bottom water in the Romanche Fracture Zone and the Chain Fracture Zone, *Journal of Physical Oceanography*, *28,* No. 5, 779–790, **Crossref**

Mercier, H., P. Morin (1997), Hydrography of the Romanche and Chain fracture zones, *Journal of Geophysical Research: Oceans*, *102,* No. C5, 10,373–10,389, **Crossref**

Molinari, R. L., R. A. Fine, E. Johns (1992), The deep western boundary current in the tropical North Atlantic Ocean, *Deep Sea Research Part A. Oceanographic Research Papers*, *39,* No. 11–12, 1967–1984, **Crossref**

Morozov, E. G. (1995), Semidiurnal internal wave global field, *Deep Sea Research Part I: Oceanographic Research Papers*, *42,* No. 1, 135–148, **Crossref**

Morozov, E. G., R. Yu. Tarakanov (2014), The Flow of Antarctic Bottom Water from the Vema Channel to the Brazil Basin, *Doklady Earth Sciences*, *456,* No. 2, 227–230, **Crossref**

Morozov, E. G., A. N. Demidov, R. Yu. Tarakanov (2008), Transport of Antarctic waters in the deep channels of the Atlantic Ocean, *Doklady Earth Sciences*, *423,* No. 1, 1286, **Crossref**

Morozov, E. G., A. N. Demidov, et al. (2010), *Abyssal Channels in the Atlantic Ocean: Water Structure and Flows*, Springer Science & Business Media, **Crossref**

Morozov, E. G., R. Y. Tarakanov, et al. (2012), Abyssal cataracts in the Romanche and Chain fracture zones, *Doklady Earth Sciences*, *446,* No. 2, 1211, **Crossref**

Morozov, E. G., R. Yu. Tarakanov, H. van Haren (2013), Transport of AABW through the Kane Gap, tropical NE Atlantic Ocean, *Ocean Science*, *9,* 825–835, **Crossref**

Morozov, E. G., R. Y. Tarakanov, N. I. Makarenko (2015), Flows of Antarctic bottom water through

fractures in the southern part of the North Mid-Atlantic Ridge, *Oceanology*, *55,* No. 6, 796–800, **Crossref**

Morozov, E. G., R. Y. Tarakanov, et al. (2017), Flows of bottom water in fractures of the North Mid-Atlantic Ridge, *Doklady Earth Sciences*, *474,* No. 2, 653–656, **Crossref**

Morozov, E. G., R. Y. Tarakanov, et al. (2018), Bottom water flows in the tropical fractures of the Northern Mid-Atlantic Ridge, *Journal of Oceanography*, *74,* No. 2, 147–167, **Crossref**

Morozov, E. G., R. Yu. Tarakanov, D. I. Frey (2021), *Bottom Gravity Currents and Overflows in Deep Channels of the Atlantic Ocean. Observations, Analysis, and Modeling*, 483 pp. Springer International Publishing, **Crossref**

Pushcharovsky, Yu. M., Yu. N. Raznitsin (1991), *Structure of the Doldrums Fracture Zone, Central Atlantic*, 224 pp. Nauka, Moscow. (in Russian)

QGIS Development Team (2021), Bottom water flows in the tropical fractures of the Northern Mid-Atlantic Ridge, QGIS, CC BY-SA. (http://qgis.osgeo.org)

Rhein, M., L. Stramma, G. Krahmann (1998), The spreading of Antarctic bottom water in the tropical Atlantic, *Deep Sea Research Part I: Oceanographic Research Papers*, *45,* No. 4–5, 507–527, **Crossref**

Rhein, M., L. Stramma, U. Send (1995), The Atlantic deep western boundary current: Water masses and transports near the equator, *Journal of Geophysical Research: Oceans*, *100,* No. C2, 2441–2457, **Crossref**

Seabrooke, J. M., G. L. Hufford, R. B. Elder (1971), Formation of Antarctic bottom water in the Weddell Sea, *Journal of Geophysical Research*, *76,* No. 9, 2164–2178, **Crossref**

Tozer, B., D. T. Sandwell, et al. (2019), *Global bathymetry and topography at 15 arc seconds: SRTM 15+, Accepted Earth and Space Science (accessed on 20.01.2021)*, (https://topex.ucsd.edu/cgi-bin/get_srtm15.cgi)**Crossref**

Troupin, C., A. Barth, et al. (2012), Generation of analysis and consistent error fields using the Data Interpolating Variational Analysis (DIVA), *Ocean Modelling*, *52–53,* 90–101, **Crossref**

Troupin, C., F. Machin, et al. (2010), High-resolution climatology of the northeast Atlantic using Data-Interpolating Variational Analysis (DIVA), *Journal of Geophysical Research: Oceans*, *115,* C8, **Crossref**

van Rossum, G., F. L. Drake, Jr. (1995), *Python Tutorial (Vol. 620)*, Centrum voor Wiskunde en Informatica, Amsterdam.

Vangriesheim, A. (1980), Antarctic bottom water flow through the Vema fracture zone, *Oceanologica Acta*, *3,* No. 2, 199–207.

Whitehead, J. A. (1998), Topographic control of oceanic flows in deep passages and straits, *Reviews of Geophysics*, *36,* No. 3, 423–440, **Crossref**

Whitehead, J. A., L. V. Worthington (1982), The flux and mixing rates of Antarctic Bottom Water within the North Atlantic, *Journal of Geophysical Research: Oceans*, *87,* No. C10, 7903–7924, **Crossref**

WHP (2002), *WOCE Hydrographic Programme, WHP: Physical oceanography during L'ATALANTE cruise 35A3CITHER1_2 on section A06. PANGAEA*, **Crossref**

Corresponding author:
I. Yu. Dudkov, Shirshov Institute of Oceanology RAS, 36, Nahimovskiy Pr., 117997 Moscow, Russia. (idudkov96@gmail.com)